

Delocalization of electrons by cavity photons in transport through a quantum dot molecule

Nzar Rauf Abdullah,^{1,*} Chi-Shung Tang,^{2,†} Andrei Manolescu,³ and Vidar Gudmundsson^{1,‡}

¹*Science Institute, University of Iceland, Dunhaga 3, IS-107 Reykjavik, Iceland*

²*Department of Mechanical Engineering, National United University, 1, Lienda, Miaoli 36003, Taiwan*

³*Reykjavik University, School of Science and Engineering, Menntavegur 1, IS-101 Reykjavik, Iceland*

We present new results on cavity-photon-assisted electron transport through two lateral quantum dots embedded in a finite quantum wire. The double quantum dot system is weakly connected to two leads and strongly coupled to a single quantized photon cavity mode with initially two linearly polarized photons in the cavity. Including the full electron-photon interaction, the transient current controlled by a plunger-gate in the central system is studied by using quantum master equation. Without a photon cavity, two resonant current peaks are observed in the range selected for the plunger gate voltage: The ground state peak, and the peak corresponding to the first-excited state. The current in the ground state is higher than in the first-excited state due to their different symmetry. In a photon cavity with the photon field polarized along or perpendicular to the transport direction, two extra side peaks are found, namely, photon-replica of the ground state and photon-replica of the first-excited state. The side-peaks are caused by photon-assisted electron transport, with multiphoton absorption processes for up to three photons during an electron tunneling process. The inter-dot tunneling in the ground state can be controlled by the photon cavity in the case of the photon field polarized along the transport direction. The electron charge is delocalized from the dots by the photon cavity. Furthermore, the current in the photon-induced side-peaks can be strongly enhanced by increasing the electron-photon coupling strength for the case of photons polarized along the transport direction.

PACS numbers: 73.23.-b, 42.50.Pq, 73.21.Hb, 78.20.Jq

I. INTRODUCTION

An opto-electronic device provides a different platform of electron transport, namely photon-assisted transport (PAT)¹. In the PAT, the energy levels of an electronic system have to match to photon frequency of a radiation source to control the electron motion. Therefore, the photon emission and the photon absorption processes play an essential role to enhance electron transport.² For that purpose, an electrostatic potential produced by a plunger-gate is applied to the electronic system to shift its energy levels in and out of resonance. The plunger-gate is widely used to control charge current³, thermal current⁴, photo-current⁵ and spin-dependent current⁶ for various quantized systems coupled to photon radiation.

The PAT controlled by plunger-gate has been investigated to study electrical⁷ and optical^{8,9} properties of a double-quantum dot (DQD) system, in which the PAT can be used as a spectroscopic tool in two different regimes defined by a zero¹⁰, and non-zero¹¹ bias voltage. At zero-bias voltage, the DQD works as a proper electron pumping device in which the photon absorption process leads to electron tunneling producing a dc current. In the non-zero bias voltage, both the photon absorption and the photon emission processes generate a dc current. Recently, both regimes have been realized experimentally in a DQD system at low temperature.^{12,13}

The most important application of a DQD system in the quantum regime is intended for information storage in a quantum state,¹⁴ quantum-bits for quantum computing,^{15,16} and quantum information processing in

two-state system.¹⁷ Recent experimental work has focused on using the two lowest energy states contributing to tunneling processes in a DQD working as a two state system: The ground state resonance, and a photon-induced excited state resonance. They observed multiphoton absorption processes up to the four-order contributing to the electron transport.¹³

Based on the above-mentioned considerations, we analyze PAT in serial double quantum dots embedded in a quantum wire. The DQD system is connected to two leads and coupled to a photon cavity with linearly polarized photons in the x - and y -directions, where the transport along the quantum wire is in the x -direction. A quantum master equation (QME) formalism is utilized to investigate transient transport of electrons controlled by the plunger-gate in the system without and with a single-photon mode.³ Generally, there are two types of QME when characterized according to memory effects, energy-dependent coupling, and the system-leads coupling strength: The Markovian and the non-Markovian QME. In the case of the Markovian approximation, the system-leads coupling is assumed weak and independent of energy, memory effect are ignored and most commonly a steady state is sought.¹⁸⁻²¹ In the non-Markovian approach, the system is energetically coupled to the leads including memory effect in the system.²²⁻²⁴ Since we are interested in studying transient transport of electrons in a regime with possible resonances, the non-Markovian model is used in our system.²⁵

In addition, we assume the DQD system to be connected to the leads through a non-zero or small bias win-

dow, where the two lowest energy states of the QDQ system can be isolated in the bias window: The ground state and the first-excited state. Our model of the DQD system can be seen as a qubit. In which the states $|0\rangle$ and $|1\rangle$ can be represented in terms of the ground state and the first-excited state. We will show how the single-photon mode affects the electron transport through both states when located in the bias window and demonstrate the role of photon activated states in the transient current. The double serial quantum dot is essential here: The two lowest single-electron states of the dot molecule have very different symmetry. The ground state has a symmetric wavefunction, but the excited state has an antisymmetric one. The conduction through the ground state is thus higher than through the excited one. The “inter-dot tunneling” can be influenced by a photon mode polarized in the transport direction, thus strongly modifying the conduction through the photon replicas of the states in a photon cavity. The nontrivial details of this picture will be analyzed in this paper reminding us that the effects rely on the geometry of the system and states beyond the ground state and the first excited one.

The rest of the paper is organized as follows. In Sec. II we introduce the model to describe the electron transport through a DQD embedded in a quantum wire connected to two leads and a photon cavity. Section. III contains two subsections, the system without and with the photon cavity. In the absence of the photon cavity, the transient current through the system controlled by the plunger-gate is demonstrated in the presence of the electron-electron interactions in the DQD system. In the photon cavity, the photon-assisted electron transport in the system is presented for a system initially with no electron, but with two linearly polarized photons in the single-photon mode. Finally, conclusions are provided in Sec. IV.

II. MODEL AND COMPUTATIONAL METHODS

The aim of this study is to model a photon-assisted electron transport in a DQD system connected to two identical electron reservoirs (lead) and coupled to a single photon mode in a cavity. Our first step is to look at the central system, in which electrons are confined in two dimensions. We assume a finite quantum wire with hard-wall ends at $x = \pm L_x/2$ with length $L_x = 165$ nm. It is parabolically confined in the y -direction (perpendicular to the transport direction) with transverse confinement energy $\hbar\Omega_0 = 2.0$ meV. The embedded quantum dots are modeled by two identical Gaussian potentials in the quantum wire defined as

$$V_{\text{DQD}}(x, y) = \sum_{i=1}^2 V_i \exp[-\beta_i^2 ((x - x_i)^2 + y^2)], \quad (1)$$

with quantum-dot strength $V_{1,2} = -2.8$ meV, $x_1 = 35$ nm, $x_2 = -35$ nm, and $\beta_{1,2} = 5.0 \times 10^{-2} \text{ nm}^{-1}$ such

that the radius of each quantum-dot is $R_{\text{QD}} \approx 20$ nm. A sketch of the DQD system under investigation is shown in Fig. 1. We should mention that the distance between the dots is $L_{\text{DQD}} = 35 \text{ nm} \simeq 1.47a_w$, and each dot is $25 \text{ nm} = 1.05a_w$ away from the nearest lead, where a_w is the effective magnetic length.

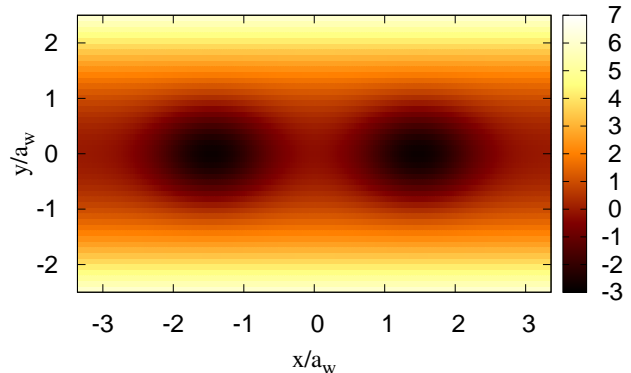


FIG. 1. (Color online) Schematic diagram depicts the potential representing the DQD embedded in a quantum wire with parameters $B = 0.1$ T, $a_w = 23.8$ nm, and $\hbar\Omega_0 = 2.0$ meV.

The DQD system is in a rectangular photon cavity with a single photon mode. The photons in the single photon mode are linearly polarized in the x - or y -directions, meaning that the photon polarization in the cavity is assumed to be parallel or perpendicular to the transport direction with respect to the electric field

$$\mathbf{A}_{\text{ph}} = A_{\text{ph}} (a + a^\dagger) \hat{\mathbf{e}}, \quad (2)$$

where A_{ph} is the amplitude of the photon vector potential, $a^\dagger(a)$ are the creation (annihilation) operators for a photon, respectively, and $\hat{\mathbf{e}}$ determines the polarization with

$$\hat{\mathbf{e}} = \begin{cases} (e_x, 0), & \text{TE}_{011} \\ (0, e_y), & \text{TE}_{101}, \end{cases}$$

where TE_{011} (TE_{101}) indicates the parallel (perpendicular) polarized photon in the transport direction, respectively.

In the following sections, we shall couple the DQD system to both the photon cavity and the leads.

A. DQD system coupled to Cavity

We consider the closed DQD system to be strongly coupled to a photon cavity. The many-body (MB) Hamiltonian

$$H_S = H_{\text{DQD}} + H_{\text{Cavity}} + H_{\text{Int}} \quad (3)$$

consists of the Hamiltonian for the closed DQD system with the electron-electron interaction H_{DQD} , the free

photon cavity Hamiltonian H_{Cavity} , and the Hamiltonian for the electron-photon interaction H_{Int} .

The DQD system (and the external leads) is placed in an external uniform perpendicular magnetic field $B\hat{z}$ in the z -direction defining an effective lateral confinement length $a_w = (\hbar/m^* \sqrt{(\omega_c^2 + \Omega_0^2)})^{1/2}$, where the effective electron mass is $m^* = 0.067m_e$ for GaAs material and $\omega_c = eB/m^*c$ is the cyclotron frequency. The Hamiltonian for the DQD system in a magnetic field including the electron-electron interaction can be written as

$$H_{\text{DQD}} = \sum_{i,j} \langle \psi_i | \left\{ \frac{\pi_e^2}{2m^*} + V_{\text{DQD}} + eV_{\text{pg}} \right\} | \psi_j \rangle \delta_{i,j} d_i^\dagger d_j + H_{\text{Coul}} + H_Z, \quad (4)$$

where $|\psi_i\rangle$ stands for a single-electron states, V_{pg} is the the plunger gate potential that shifts the energy levels of the DQD system with respect to the chemical potentials of the leads, d_i^\dagger (d_j) is an operator that creates (annihilates) an electron in the DQD system, respectively. Moreover, the canonical momentum is $\pi_e = \mathbf{p} + \frac{e}{c}\mathbf{A}_{\text{ext}}$ with the kinetic momentum operator \mathbf{p} , and the vector potential in the Landau gauge $\mathbf{A}_{\text{ext}} = (0, -By, 0)$. The electron-electron interaction in the central system is given by

$$H_{\text{Coul}} = \frac{1}{2} \sum_{ijrs} V_{ijrs} d_i^\dagger d_j^\dagger d_s d_r, \quad (5)$$

with the Coulomb matrix elements V_{ijrs} .²⁶ The characteristic Coulomb energy is $E_C = e^2/(2\epsilon_r a_w) \approx 2.44$ meV at $B = 0.1$ T with $a_w = 23.8$ nm and $\epsilon_r = 12.4$, the dielectric constant of GaAs. The characteristic Coulomb energy is greater than the thermal energy of the leads. An exact numerical diagonalization method is used here for solving the Coulomb interacting many-electron (ME) Hamiltonian in a truncated Fock space to obtain the ME energy spectrum of the DQD system.²⁷ The Zeeman Hamiltonian shown in the third part of Eq. (4) describes the interaction between the external magnetic field and the magnetic moment of an electron

$$H_Z = \pm \frac{g^* \mu_B}{2} B, \quad (6)$$

where \pm stands for z -spin components, $\mu_B = e\hbar/2m_e c$ is the Bohr magneton, and the effective Lande g -factor is $g^* = -0.44$ for GaAs.

In order to investigate photon-assisted electron transport in the DQD system, the electronic system is coupled to a photon cavity. The Hamiltonian of the free photon cavity is given by

$$H_{\text{Cavity}} = \hbar\omega_{\text{ph}} \hat{N}_{\text{ph}}, \quad (7)$$

where $\hbar\omega_{\text{ph}}$ is the energy of the single mode in the cavity, and $\hat{N}_{\text{ph}} = a^\dagger a$ is the photon number operator. The interaction of the single quantized electromagnetic mode with the electronic system is described by the Hamiltonian

including both the diamagnetic and the paramagnetic interactions of photons and electrons

$$H_{\text{Int}} = g_{\text{ph}} \sum_{ij} d_i^\dagger d_j g_{ij} \{a + a^\dagger\} + \frac{g_{\text{ph}}^2}{\hbar\Omega_w} \sum_i d_i^\dagger d_i \left[\hat{N}_{\text{ph}} + \frac{1}{2} (a^\dagger a^\dagger + aa + 1) \right] \quad (8)$$

herein, $g_{\text{ph}} = eA_{\text{ph}}\Omega_w a_w/c$ is the electron-photon coupling strength, and g_{ij} are dimensionless electron-photon coupling matrix elements.²⁸

Finally, the MB system Hamiltonian H_S is diagonalized in a MB Fock-space $\{|\check{\alpha}\rangle\}$ to obtain the MB energy spectrum of the DQD system coupled to the photon cavity.²⁹ The diagonalization builds a new interacting MB state basis $\{|\check{\nu}\rangle\}$, in which $|\check{\nu}\rangle = \sum_\alpha \mathcal{W}_{\mu\alpha} |\check{\alpha}\rangle$ with $\mathcal{W}_{\mu\alpha}$ being a unitary transformation matrix. The unitary transformation is used to convert the QME and the physical observables from non-interacting MB basis to the interacting MB basis.

B. DQD system connected to leads

The DQD system is connected to two semi-infinite leads with the same width. The chemical potential of the lead l is μ_l , with $l \in \{L, R\}$ being the left L and the right R lead. The the Fermi function in the isolated lead l before coupling to the central system is $f_l(\epsilon_l(\mathbf{q})) = \{\exp[\epsilon_l(\mathbf{q}) - \mu_l] + 1\}^{-1}$, where ϵ_l is the SE subband energy of the lead l (\mathbf{q} is the momentum dummy index.³) found from the non-interacting ME Hamiltonian of lead l

$$H_l = \int d\mathbf{q} \epsilon_l(\mathbf{q}) c_{\mathbf{q}l}^\dagger c_{\mathbf{q}l}, \quad (9)$$

with $c_{\mathbf{q}l}^\dagger$ ($c_{\mathbf{q}l}$) the electron creation(annihilation) operator in lead l , respectively.³⁰

In order to instigate electron transport between the subsystems, the DQD system is coupled to the leads with energy dependent coupling coefficients reflecting the geometry of the system

$$T_{\mathbf{q}il} = \int d\mathbf{r} d\mathbf{r}' \psi_{\mathbf{q}l}(\mathbf{r}')^* g_{\mathbf{q}il}(\mathbf{r}, \mathbf{r}') \psi_i^S(\mathbf{r}). \quad (10)$$

An electron may be transferred from a state $|\mathbf{q}\rangle$ with the wavefunction $\psi_{\mathbf{q}l}(\mathbf{r}')$ in the leads to a SE state $|i\rangle$ with the SE wavefunction $\psi_i^S(\mathbf{r})$ in the DQD system and vice versa, where the coupling function is $g_{\mathbf{q}il}(\mathbf{r}, \mathbf{r}')$.²⁵ The coupling coefficients are utilized to construct a time-dependent coupling Hamiltonian in the second quantization language

$$H_{\text{TI}}(t) = \chi_I(t) \sum_i \int d\mathbf{q} \left[c_{\mathbf{q}l}^\dagger T_{\mathbf{q}il} d_i + d_i^\dagger (T_{i\mathbf{q}l})^* c_{\mathbf{q}l} \right], \quad (11)$$

with a time-dependent switching function $\chi_l(t) = 1 - 2\{\exp[\alpha_l(t-t_0)]+1\}^{-1}$ with $\alpha_l = 0.3 \text{ ps}^{-1}$ being a switching parameter.

After the DQD system is coupled to the leads at $t = 0$, we calculate the time evolution of the electrons and photons using the density operator and its equation of motion, the Liouville-von Neumann (Lv-N) equation $i\hbar\dot{W}(t) = [H(t), W(t)]$ for the whole system. As this can not be accomplished we resort to using a projection formalism taking a trace over the Hilbert space of the leads introducing the reduced density operator

$$\rho(t) = \text{Tr}_L \text{Tr}_R W(t) \quad (12)$$

with $\rho(t_0) = \rho_S^{31}$ and the condition that $W(t < t_0) = \rho_L \rho_R \rho_S$ is the density operator of the total system before the coupling with ρ_S being the density operator of the isolated DQD system.³² The density operator of the leads before the coupling is $\rho_l = \exp[-\beta(H_l - \mu_l N_l)] / \text{Tr}_l \{\exp[-\beta(H_l - \mu_l N_l)]\}$, where $\beta = 1/k_B T_l$ is the inverse thermal energy, and N_l is the number operator for electrons in the lead l ,³⁰

The time-dependent mean charge in the central system, the current in the leads are calculated from the reduced density operator as has been detailed in earlier publications.^{3,29}

III. NUMERICAL RESULTS

In this section, we discuss the transport properties through the DQD system controlled by plunger-gate voltage in both cases without a photon cavity and with x - or y -polarized photons in a cavity.

In order to obtain the PAT, the system has to satisfy the following conditions: the MB energy level spacing has to be greater than the thermal energy $\Delta E_{\text{MB}} > k_B T$, and the MB energy level spacing has to be smaller or equal to the photon energy $\Delta E_{\text{MB}} \leq \hbar\omega_{\text{ph}}$.³³ Initially the temperature of the central system is assumed to be $T = 0 \text{ K}$, and the leads are at $T = 0.01 \text{ K}$ initially. Other physical parameters of the system are presented in table I.

Quantity	Typical parameter
Thermal energy in leads ($k_B T$)	$\approx 8.617 \times 10^{-4} \text{ meV}$
Characteristic Coulomb energy (E_C)	$\approx 2.44 \text{ meV}$
Photon energy ($\hbar\omega_{\text{ph}}$)	$= 0.25 \text{ meV}$

TABLE I. Characteristic energy scales of the system

In addition, we assume the external magnetic field to be $B = 0.1 \text{ T}$ with the effective lateral confinement length $a_w = 23.8 \text{ nm}$ and initially no electron is in the DQD system.

A. The DQD system without the photon cavity

In this section, the properties of the electron transport through the DQD system are presented in the absence of the photon cavity in order to establish a comparison for later results for transport through the system inside a cavity.

Figure 2(a) shows the energy spectrum of the leads versus wave number qa_w . The horizontal black lines are chemical potentials of the left lead μ_L and the right lead μ_R . The chemical potentials are considered to be $\mu_L = 1.4 \text{ meV}$ and $\mu_R = 1.3 \text{ meV}$, implying a small bias voltage $\Delta\mu = 0.1 \text{ meV}$. Therefore, the first subband in the parabolic energy spectrum becomes the most active subband contributing to the electron transport process in the energy range $[1.3, 1.4] \text{ meV}$.

In Fig. 2(b), the ME energy spectrum of the DQD-system as a function of applied plunger-gate voltage V_{pg} is shown. The energies of two-electron states $N_e = 2$ (2ES, blue dots) are higher than the SE states $N_e = 1$ (1ES, red dots) due to the electron-electron interaction. In the absence of the photon cavity, two resonant SE states are situated in the bias window for the range of plunger gate voltage selected here, namely, the ground state resonance and first-excited state resonance (blue squared dots).

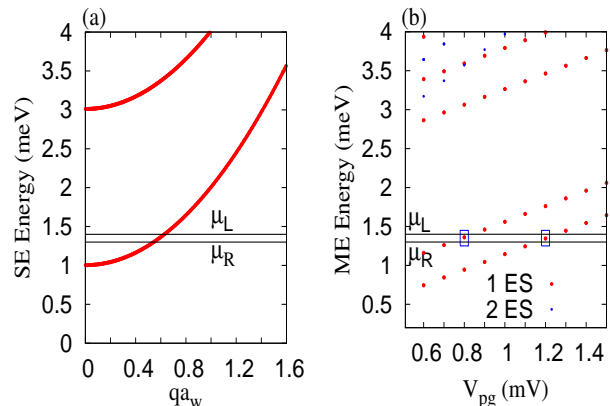


FIG. 2. (Color online) Energy spectra in the case of no photon cavity with magnetic field $B = 0.1 \text{ T}$. (a) SE energy spectrum in the leads (red) is plotted as a function of scaled wave number qa_w , where the chemical potentials are $\mu_L = 1.4 \text{ meV}$ and $\mu_R = 1.3 \text{ meV}$ (black). (b) ME energy spectrum in the central system as a function of plunger gate voltage V_{pg} including SE states (1ES, red dots) and two electron states (2ES, blue dots). The SE state in the bias window is almost doubly degenerate due to the small Zeeman energy.

The almost degenerate two spin states of the single-electron ground state are $|2\rangle$ and $|3\rangle$ with energies $E_2 = 1.343 \text{ meV}$ and $E_3 = 1.346 \text{ meV}$. These two states get into resonance with the first-subband of the leads at $V_{\text{pg}}^{\text{G}} = 1.2 \text{ mV}$, where the superscript G refers to the ground state. By tuning the plunger-gate voltage, the two spin states of the first-excited state $|4\rangle$ and $|5\rangle$ with

energies $E_4 = 1.358$ meV and $E_5 = 1.361$ meV contribute to the electron transport at $V_{\text{pg}}^{\text{FE}} = 0.8$ mV, where the superscript FE stands for the first-excited state.

Figure 3 displays the left current I_L (red solid) and the right current I_R (dashed blue) through the DQD system. We notice two resonance peaks in the currents: The

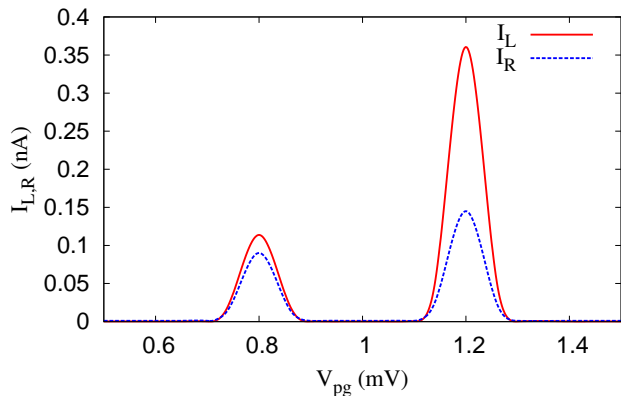


FIG. 3. (Color online) The left current I_L (red solid) and right current I_R (blue dashed) are plotted as a function of plunger gate voltage V_{pg} at time $t = 220$ ps in the case of no photon cavity. Other parameters are $B = 0.1$ T and $\Delta\mu = 0.1$ meV.

ground state peak at $V_{\text{pg}}^{\text{G}} = 1.2$ mV and the first-excited state peak at $V_{\text{pg}}^{\text{FE}} = 0.8$ mV. The reason for the two current peaks is resonance of the SE states in the DQD system with the first subband energy of the leads. An electron in the first-subband of the left lead may tunnel to the state $|2\rangle$ or $|3\rangle$ of the DQD system and subsequently tunnel out to the right lead. Consequently the ground state peak is observed at $V_{\text{pg}}^{\text{G}} = 1.2$ mV. In addition, the first-excited state peak reflects a resonance with the states $|4\rangle$ and $|5\rangle$ at plunger-gate potential $V_{\text{pg}}^{\text{FE}} = 0.8$ mV.

Figure 4 shows the charge density distribution in the DQD system at time $t = 220$ ps (after the initial transient, close to a steady state) in the ground state peak (a), and the first-excited state peak (b). In the case of the ground state peak at $V_{\text{pg}}^{\text{G}} = 1.2$ mV, the electron state accumulates in the dots with a strong inter-dot tunneling. Therefore, the left and right currents increase in the system. But in the case of first-excited state peak at $V_{\text{pg}}^{\text{FE}} = 0.8$ mV, the electron state is strongly localized in the dots without much tunneling between the dots. Thus the tunneling between the dots is sufficiently suppressed and the current drops as shown in Fig. 3.

B. x -photon polarization (TE_{011} mode)

In this section we analyze the electron transport through the DQD system in the presence of an x -polarized single-photon mode with initially two photons

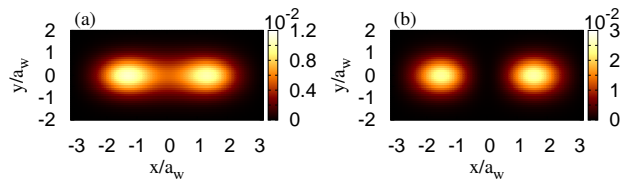


FIG. 4. (Color online) The charge density distribution at $t = 220$ ps in the ground state peak (a) and first-excited state peak (b) shown in Fig. 3 in the case with no photon cavity. Other parameters are $B = 0.1$ T, $a_w = 23.8$ nm, $L_x = 165$ nm $= 6.93a_w$, and $\Delta\mu = 0.1$ meV.

in the cavity. The photons in the cavity can excite electrons in the DQD system and enhance the electric current, similar to the “classical” PAT case.¹¹ The condition for PAT involving N_{ph} photon(s) is $|E_i - E_f| = N_{\text{ph}}\hbar\omega_{\text{ph}}$,³⁴ where E_i (E_f) is the highest possible initial (lowest possible final) MB energy level of the DQD system, respectively.³³ We vary the applied plunger-gate to match $|E_i - E_f|$ to the photon energy, thus the PAT is an active process in the system.

Figure 5 shows the MB energy spectrum of the DQD system including the photons with zero-electron states $N_e = 0$ (0ES, green dots) and SE states $N_e = 1$ (1ES, red dots). In addition to the former states at

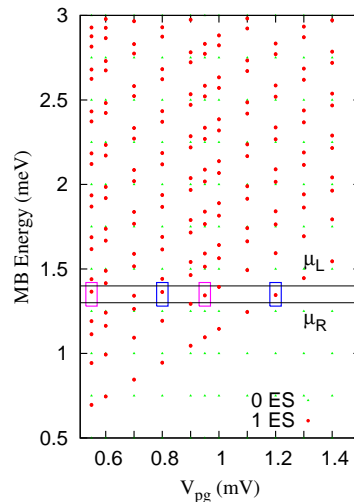


FIG. 5. (Color online) MB Energy spectrum versus the plunger gate voltage V_{pg} in the case of x -polarized photon field, where 0ES indicates zero electron states ($N_e = 0$, green dots), and 1ES stands for single electron states ($N_e = 1$, red dots). Other parameters are $B = 0.1$ T, $\Delta\mu = 0.1$ meV, and $\hbar\omega_{\text{ph}} = 0.25$ meV.

$V_{\text{pg}}^{\text{G}} = 1.2$ mV and $V_{\text{pg}}^{\text{FE}} = 0.8$ mV, two extra active MB-states are observed in the presence of the photon cavity at $eV_{\text{pg}}^{\text{G};\text{FE}} = eV_{\text{pg}}^{\text{G};\text{FE}} - \hbar\omega_{\text{ph}}$ in the bias window (pink squared dots), where the photon energy is

$\hbar\omega_{\text{ph}} = 0.25$ meV, and $G_\gamma(\text{FE}_\gamma)$ stands for the photon-replica of the ground state(first-excited state), respectively. We notice that all states in the bias window are SE states containing only one-electron $N_e = 1$.

Figure 6 displays the left current I_L (a) and the right current I_R (b) as a function of the plunger-gate voltage V_{pg} in the presence of the x -polarized photon field at time $t = 220$ ps for different electron-photon coupling strength $g_{\text{ph}} = 0.1$ meV (blue solid), 0.2 meV (green dashed), and 0.3 meV (red dotted). The positive value of the left current indicates electrons tunneling from the left lead to the DQD system, while the negative value of the right current denotes electrons tunneling from the right lead to the DQD system and vice versa.

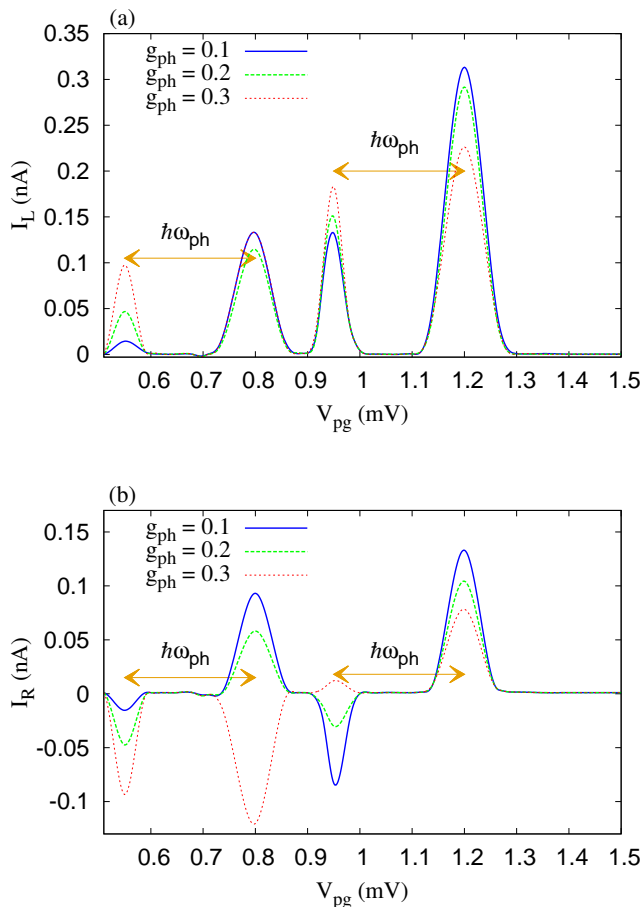


FIG. 6. (Color online) The left current I_L (a), and the right current I_R (b) versus the plunger gate voltage V_{pg} in the case of x -polarized photon field at time $t = 220$ ps with different electron-photon coupling strength: $g_{\text{ph}} = 0.1$ meV (blue solid), 0.2 meV (green dashed), and 0.3 meV (red dotted). Other parameters are $\hbar\omega_{\text{ph}} = 0.25$ meV, $\Delta\mu = 0.1$ meV, and $B = 0.1$ T.

In the absence of the photon cavity, two main-peaks are found at $V_{\text{pg}}^{\text{FEM}} = 0.8$ mV and $V_{\text{pg}}^{\text{GM}} = 1.2$ mV as shown in Fig. 3. In the presence of the photon cavity, two extra side-peaks at $eV_{\text{pg}}^{\text{GS};\text{FES}} = eV_{\text{pg}}^{\text{GM};\text{FEM}} - \hbar\omega_{\text{ph}}$

are observed in addition to the original main-peaks at $V_{\text{pg}}^{\text{GM};\text{FEM}}$. The superscripts GM(FEM) refers to the ground states(first-excited state) main-peak, respectively, and GS(FES) stands for photon-induced ground state(first-excited state) side-peak, respectively.

The side-peaks indicate the PAT, where the system satisfies $e|V_{\text{pg}}^{\text{GM};\text{FEM}} - V_{\text{pg}}^{\text{GS};\text{FES}}| \cong \hbar\omega_{\text{ph}}$.³³ The two new side-peaks at $V_{\text{pg}}^{\text{GS}} = 0.95$ mV and $V_{\text{pg}}^{\text{FES}} = 0.55$ mV shown in Fig. 6 are caused by photon-replica of the ground state and photon-replica of the first-excited state, respectively. We find that the separation of the photon replica side-peaks from the original main-peaks corresponds to the photon energy.

It should be noted that the current in the photon-induced side-peaks is strongly enhanced by increasing the electron-photon coupling strength. Thus the photon-induced side-peaks exhibits a PAT process with different photon absorption mechanism from the main-peaks.

In order to show the dynamics of the PAT process involved in the formation of the photon-induced side-peaks in the left and right current shown in figure 6, we schematically present the photon absorption process in Fig. 7.

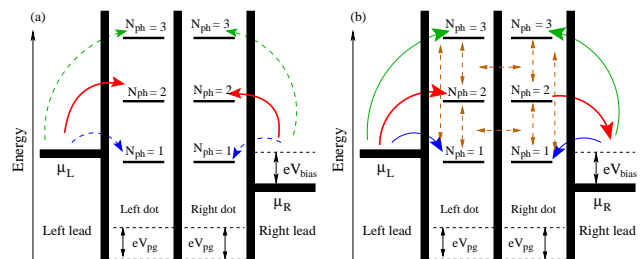


FIG. 7. (Color online) Schematic representation of photon-activated resonance energy levels and electron transition by changing the plunger gate voltage V_{pg} in the photon-induced first-excited state side-peak at $V_{\text{pg}}^{\text{FES}} = 0.55$ mV (a), and the photon-induced ground state side-peak at $V_{\text{pg}}^{\text{GS}} = 0.95$ mV(b) of the Fig. 6. The DQD-system is embedded in a photo cavity with the photon energy $\hbar\omega_{\text{ph}}$ and photon content N_{ph} in each many-body state. The chemical potential difference is $eV_{\text{bias}} = \Delta\mu = \mu_L - \mu_R$.

Figure 7(a) demonstrates the tunneling processes forming the FES at $V_{\text{pg}}^{\text{FES}} = 0.55$ mV. The electron from the left or the right lead absorbs two photons and is transferred to the MB states containing two photons $N_{\text{ph}} = 2$ (red solid arrows) situated above the bias window with photon energy $\hbar\omega_{\text{ph}}$. The electron tunneling process in the states containing one photon $N_{\text{ph}} = 1$ (blue dashed arrows) and three photons $N_{\text{ph}} = 3$ (green dashed arrows) are very weak. Figure 7(b) shows the dynamical mechanism that makes the GS at $V_{\text{pg}}^{\text{GS}} = 0.95$ mV. In addition to the electron tunneling in the state containing two photons $N_{\text{ph}} = 2$ (red solid arrows), the tunneling process in one photon state $N_{\text{ph}} = 1$ (blue solid arrows) and three photons $N_{\text{ph}} = 3$ states (green solid arrows) become active. The tunneling mechanism here is a mul-

tiphoton absorption process with up to three photons with a strong inter-dot tunneling. In which the electron is scattered between one, two, and three photon(s) states by absorbing and emitting photon energy $N_{\text{ph}} \times \hbar\omega_{\text{ph}}$. The two photons state here has a shorter lifetime than the two photons states in the FES, because whenever an electron from the left lead tunnels into the two photon states in the DQD system it subsequently directly tunnels out to the right lead.

To further illustrate the characteristics of the most active MB states in the tunneling process forming the two main current peaks and the two side current peaks in the Fig. 6, we present Fig. 8 which shows the characteristics of the MB states at plunger-gate voltage $V_{\text{pg}}^{\text{FES}} = 0.55$ mV (a), $V_{\text{pg}}^{\text{FEM}} = 0.8$ mV (b), $V_{\text{pg}}^{\text{GS}} = 0.95$ mV (c), and $V_{\text{pg}}^{\text{GM}} = 1.2$ mV (d) in the case of $g_{\text{ph}} = 0.1$ meV.

Figure 8(a) indicates how the FES is contributed to by the MB states at $V_{\text{pg}}^{\text{FES}} = 0.55$ mV. Since there are two photons initially in the cavity, we shall seek the MB-states that contain one, two, and three photon(s), to observe multiple inelastic electron scattering in the states of DQD system at the side-peaks.² Here, we focus on six MB states, two inactive MB states $|\check{15}\rangle$ and $|\check{16}\rangle$ in the bias window (blue squared dot) with $N_{\text{ph}} = 1.052$ in each state and the energies $E_{15} = 1.364$ meV and $E_{16} = 1.366$ meV. There are four MB state above the bias window: Two photon-activated states $|\check{20}\rangle$ and $|\check{21}\rangle$ (red squared dot) with $N_{\text{ph}} = 2.073$ in each state and energies $E_{20} = 1.616$ meV and $E_{21} = 1.618$ meV, and two more MB states $|\check{25}\rangle$ and $|\check{26}\rangle$ (green squared dot) with $N_{\text{ph}} = 3.094$ in each state and energies $E_{25} = 1.867$ meV and $E_{26} = 1.870$ meV. We clearly see that the energy difference between the inactive states and the photon-activated states is appropriately equal to the $(N_{\text{ph,ac}} - N_{\text{ph,in}}) \times \hbar\omega_{\text{ph}}$, where $N_{\text{ph,ac}}$ and $N_{\text{ph,in}}$ are the photon number in the photon-activated states and the inactive states, respectively. We observe that the electrons can undergo the following possible tunneling process: An electron from either lead may absorb two photons from the cavity being transferred to two photons states $|\check{20}\rangle$ and $|\check{21}\rangle$ with absorption energy $E_{20} - E_{15} = (N_{\text{ph,20}} - N_{\text{ph,15}}) \times \hbar\omega_{\text{ph}} \simeq 0.252$ meV or $E_{21} - E_{16} = (N_{\text{ph,21}} - N_{\text{ph,16}}) \times \hbar\omega_{\text{ph}} \simeq 0.252$ meV which is approximately equal to the energy required to transfer an electron from the leads to two photons states as schematically shown in Fig. 7(a). Therefore, the two photon absorption mechanism dominates here without making electron inelastic scattering to the one and three photon states. The electron tunneling process from the leads to the DQD system suggest that the electrons are collected in either individual dot.

Figure 8(b) shows the MB states of the first-excited state main-peak at $V_{\text{pg}}^{\text{FEM}} = 0.8$ mV. There are two inactive states $|\check{11}\rangle$ and $|\check{12}\rangle$ (blue squared dot) with energies $E_{11} = 1.362$ meV and $E_{12} = 1.364$ meV in the bias window ($N_e = 1$, $N_{\text{ph}} = 0.029$) and two photon-activated states $|\check{21}\rangle$, and $|\check{22}\rangle$ (red squared dot)

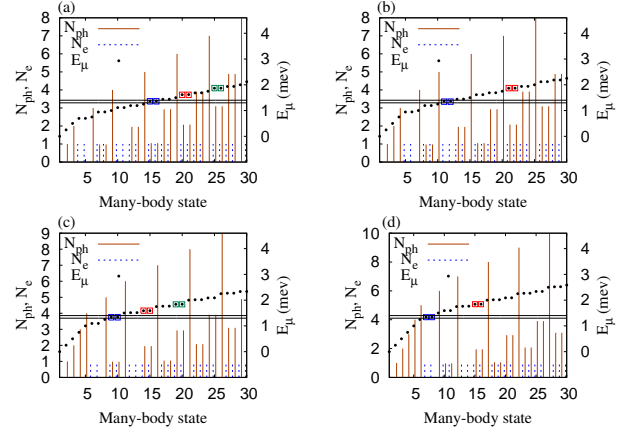


FIG. 8. (Color online) The MB energy spectrum E_{μ} (dotted black), the mean electron number in the MB state $|\check{\mu}\rangle$ (blue dashed line), the mean photon number N_{ph} (red line) in the case of x -polarized field with plunger-gate voltage at (a) photon-induced first-excited side-peak $V_{\text{pg}}^{\text{FES}} = 0.55$ mV, (b) first-excited main-peak $V_{\text{pg}}^{\text{FEM}} = 0.8$ mV, (c) photon-induced ground-state side-peak $V_{\text{pg}}^{\text{GS}} = 0.95$ mV, and (d) ground-state main-peak $V_{\text{pg}}^{\text{GM}} = 1.2$ mV of Fig. 6 for the case of $g_{\text{ph}} = 0.1$ meV (blue solid line). The chemical potentials are $\mu_L = 1.4$ meV and $\mu_R = 1.3$ meV (black line), thus $\Delta\mu = 0.1$ meV. Other parameters are $B = 0.1$ T, and $\hbar\omega_{\text{ph}} = 0.25$ meV. The color of the square is referred to in the text.

with energies $E_{21} = 1.866$ meV and $E_{22} = 1.868$ meV above the bias window ($N_e = 1$, $N_{\text{ph}} = 2.073$). The photon-activated states that contain two photons are responsible for the electron transport with energy values $E_{21} - E_{11} \simeq (N_{\text{ph,21}} - N_{\text{ph,11}}) \times \hbar\omega_{\text{ph}} \simeq 0.504$ meV or $E_{22} - E_{12} \simeq (N_{\text{ph,22}} - N_{\text{ph,12}}) \times \hbar\omega_{\text{ph}} \simeq 0.504$ meV.

Figure 8(c) demonstrates the MB states that participate to the electron transport in the GS at $V_{\text{pg}}^{\text{GS}} = 0.95$ mV. The electron transport mechanism here is different from the one for the FES. The contributions to the GS is by the following significant MB states: Two active MB states $|\check{9}\rangle$ and $|\check{10}\rangle$ (blue squared dot) containing $N_{\text{ph}} = 0.976$ with energies $E_9 = 1.342$ meV and $E_{10} = 1.344$ meV are located in the bias window, two photon-activated states $|\check{14}\rangle$ and $|\check{15}\rangle$ (red squared dot) have $N_{\text{ph}} = 1.95$ above the bias window with energies $E_{14} = 1.5901$ meV and $E_{15} = 1.5902$ meV, and two more photon-activated states $|\check{19}\rangle$ and $|\check{20}\rangle$ (green squared dot) contain $N_{\text{ph}} = 2.93$ with energies $E_{19} = 1.838$ meV and $E_{20} = 1.840$ meV. Significantly, these six MB states participate in the electron transport with the following important photon absorption processes with inter-dot tunneling as schematically shown previously in Fig. 7(b): (1) Electron from either lead absorbs one photon tunneling to the one photon states $|\check{9}\rangle$ and $|\check{10}\rangle$, (2) An electron from the left lead absorbs two photons and is transferred to two photons states $|\check{14}\rangle$ and $|\check{15}\rangle$ with absorption energy $E_{14} - E_9 = (N_{\text{ph,14}} - N_{\text{ph,9}}) \times \hbar\omega_{\text{ph}} \simeq 0.248$ meV or $E_{15} - E_{10} = (N_{\text{ph,15}} - N_{\text{ph,10}}) \times \hbar\omega_{\text{ph}} \simeq 0.247$ meV

which is approximately equal to the energy required to transfer electron from one photon state to two photons states, then the electron tunnels to the right lead emitting photons, (3) Absorbing three photons, an electrons from either the left lead or the right lead transfers to three photons states $|\check{19}\rangle$ and $|\check{20}\rangle$ with energy $E_{19} - E_9 = (N_{\text{ph},19} - N_{\text{ph},9}) \times \hbar\omega_{\text{ph}} \simeq 0.496$ meV or $E_{20} - E_{10} = (N_{\text{ph},20} - N_{\text{ph},10}) \times \hbar\omega_{\text{ph}} \simeq 0.496$ meV that is approximately the energy amount needed to transfer an electron to a three photons state. The tunneling processes from the leads to the DQD system and all activated six-MB states suggest that the electrons perform multiple scattering absorption and emission processes between the states in each individual dot with inter-dot tunneling. These possible tunneling processes indicate to us that the existence of the FES is caused by multiphoton absorption processes with up to three photons. In addition, we should mention that the tunneling process from the left lead to two photon states in the DQD system and the tunnel out to the right lead decreases the dwell time of electron in the central system, while the dwell time of electron in the FES was longer due to charge accumulation in the DQD system.

Figure 8(d) demonstrates the MB states of the ground state main-peak at $V_{\text{pg}}^{\text{GM}} = 1.2$ mV. Four MB states are also important here, two inactive states $|\check{7}\rangle$ and $|\check{8}\rangle$ (blue squared dot) with energies $E_7 = 1.344$ meV and $E_8 = 1.346$ meV in the bias window ($N_e = 1$, $N_{\text{ph}} = 0.029$) and two photon-activated states $|\check{15}\rangle$ and $|\check{16}\rangle$ (red squared dot) with energies $E_{15} = 1.840$ meV and $E_{16} = 1.842$ meV above the bias window ($N_e = 1$, $N_{\text{ph}} = 1.951$). The energy difference between photon-activated states above the bias window and the inactive states in the bias window satisfies the same rule of the FEM, such that $E_{15} - E_7 \cong (N_{\text{ph},15} - N_{\text{ph},7}) \times \hbar\omega_{\text{ph}} \cong 0.496$ meV and $E_{16} - E_8 \cong (N_{\text{ph},16} - N_{\text{ph},8}) \times \hbar\omega_{\text{ph}} \cong 0.496$ meV.

These results suggest that each photon-activated state above the bias window has two more photons than the inactive states in the bias window at both the main peaks. When an electron from the left lead tunnels to the DQD system it absorbs (or forms a quasi-particle with) two photons from the cavity and is transferred to the photon-activated states above the bias window, then it tunnels to the right lead. Therefore, both main-peaks are caused by two photons absorption processes in the transport.

Observing all these photon activated processes it is important to have in mind that the fact that we retained the dia- and the paramagnetic parts of the electron-photon interaction (Eq. (8)) thus allowing for a broader range of transitions possibilities than only the paramagnetic term describes.

Figure 9 indicates the charge density distribution in the DQD system with x -polarized photon field at plunger-gate $V_{\text{pg}}^{\text{FES}} = 0.55$ mV (a), $V_{\text{pg}}^{\text{FEM}} = 0.8$ mV (b), $V_{\text{pg}}^{\text{GS}} = 0.95$ mV (c), and $V_{\text{pg}}^{\text{GM}} = 1.2$ mV (d) of the Fig. 6 at time $t = 220$ ps and $g_{\text{ph}} = 0.1$ meV. In the FES at $V_{\text{pg}}^{\text{FES}} = 0.55$ mV, the electron charge density forms two peaks which are strongly localized in the dots without

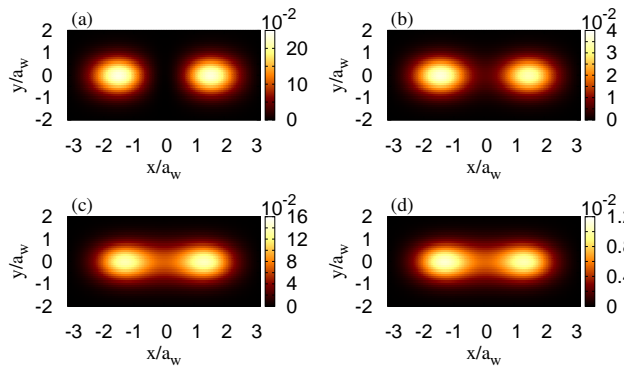


FIG. 9. (Color online) The charge density distribution of the DQD system with x -polarized photon field at time 220 ps corresponding to (a) photon-induced first-excited side-peak $V_{\text{pg}}^{\text{FES}} = 0.55$ mV, (b) first-excited main-peak $V_{\text{pg}}^{\text{FEM}} = 0.8$ mV, (c) photon-induced ground-state side-peak $V_{\text{pg}}^{\text{GS}} = 0.95$ mV, and (d) ground-state main-peak $V_{\text{pg}}^{\text{GM}} = 1.2$ mV of Fig. 6. for the case of $g_{\text{ph}} = 0.1$ meV (blue solid line). Other parameters are $\hbar\omega_{\text{ph}} = 0.25$ meV, $B = 0.1$ T, $a_w = 23.8$ nm, $L_x = 300$ nm, and $\hbar\Omega_0 = 2.0$ meV.

inter-dot tunneling shown in Fig. 9(a), thus the electron dwell time is increased and the electrons stay longer time in the DQD system.

In the case of $V_{\text{pg}}^{\text{FEM}} = 0.8$ mV, the electrons are accumulated in the dots with a weak inter-dot tunneling. Comparing to the case with no photon cavity Fig. 4(a), a slight inter-dot tunneling is observed indicating charge polarization between the dots. As a result, the electron charge density is slightly enhanced in the x -polarized photon field, but more importantly it is also slightly delocalized resulting in a higher conductance through the serial dot molecule.

In the GS at $V_{\text{pg}}^{\text{GS}} = 0.95$ mV, the electron charge density is enhanced and exhibits charge accumulation in the dots with a very strong inter-dot tunneling shown in Fig. 9(c) which decreases the electron dwell time in the DQD-system. This is the reason why the current in the GS is relatively higher than the current is FES.

In the case of $V_{\text{pg}}^{\text{GM}} = 1.2$ mV, the electron-photon interactions does not have a big effect on the charge density distribution, the charge distribution of the dots is already overlapping.

C. y -photon polarization (TE₁₀₁ mode)

In this section, we assume the photon-cavity is linearly polarized in the y -direction with photon energy $\hbar\omega_{\text{ph}} = 0.25$ meV and initially two photons in the single photon mode. The MB energy spectrum of the DQD-system in the y -polarization is very similar to that in the x -polarization photon mode as shown in Fig. 5. Two extra MB states are observed with the spin states of the ground state and first-excited state in the bias window, the extra MB states indicate the photon-replica states in

the presence of the photon cavity.

Figure 10 shows the left current (a) and the right current (b) at time $t = 220$ ps for different electron-photon coupling strength $g_{\text{ph}} = 0.1$ meV, (blue solid), 0.2 meV (green dashed), and 0.3 meV (red dotted). Similar to the x -polarized photon field, two extra photon-induced side-peaks at $V_{\text{pg}}^{\text{FES}} = 0.55$ mV and $V_{\text{pg}}^{\text{GS}} = 0.95$ mV are observed with the main-peaks at $V_{\text{pg}}^{\text{FEM}} = 0.8$ mV $V_{\text{pg}}^{\text{GM}} = 1.2$ mV. A very weak current enhancement in the photon-induced side-peaks is predicted by increasing the electron-photon coupling strength, while the current enhancement in the photon-induced side-peaks is very strong in the x -polarized photon field shown in Fig. 6. The weaker effects for the y -polarization are expected since the photon energy is farther from resonance for states describing motion in that direction, i.e. the confinement energy in the y -direction is much higher.

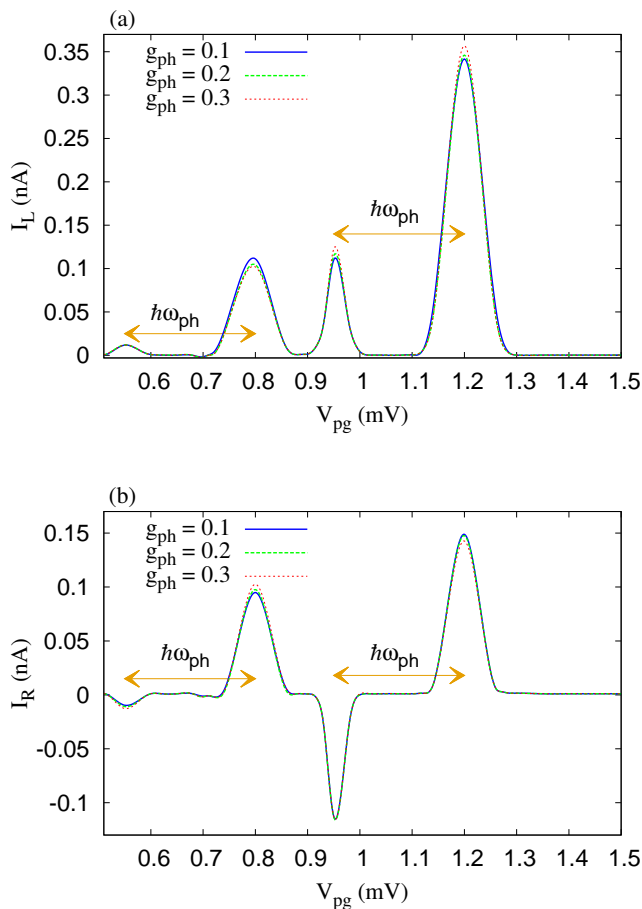


FIG. 10. (Color online) The left current (a) and the right current (b) versus the plunger gate voltage V_{pg} at time ($t = 220$ ps) in the case of y -polarized photon field. The electron-photon coupling is changed to be $g_{\text{ph}} = 0.1$ meV (blue solid), 0.2 meV (green dashed), and 0.3 meV (red dotted). Other parameters are $\hbar\omega_{\text{ph}} = 0.25$ meV, $\Delta\mu = 0.1$ meV, and $B = 0.1$ T.

The characteristics of the MB states in the bias window and above the bias window in the y -polarized photon field are very similar to that in the x -direction shown in Fig. 8. The main-peaks and the photon-induced side-peaks in the y -polarized photon are contributed to by almost the same absorption processes of the x -polarized photon.

Figure 11 demonstrates the charge density distribution in the DQD system in the case of y -polarized photon field at plunger-gate voltage $V_{\text{pg}}^{\text{FES}} = 0.55$ mV FES (a), $V_{\text{pg}}^{\text{FEM}} = 0.8$ mV FEM (b), $V_{\text{pg}}^{\text{GS}} = 0.95$ mV GS (c), and $V_{\text{pg}}^{\text{GM}} = 1.2$ mV GM (d) shown in the Fig. 10, at time $t = 220$ ps and $g_{\text{ph}} = 0.1$ meV. In the case of $V_{\text{pg}}^{\text{FES}} = 0.55$ mV (FES), the electrons are strongly localized in the dots with no electron tunneling from the left-dot to the right-dot.

In FEM at $V_{\text{pg}}^{\text{FEM}} = 0.8$ mV, the electron makes a resonance state localized in each dot without inter-dot tunneling, while a weak inter-dot tunneling was observed in the x -polarized photon field at FEM shown in Fig. 9(b). Therefore, the electron dwell time in the DQD system in y -polarized photon is longer than that in the x -polarized photon at FEM.

But at $V_{\text{pg}}^{\text{GS}} = 0.95$ mV (GS), the inter-dot tunneling is very strong and electrons prefer to make inelastic multiple scattering in each dot with inter-dot tunneling.

In GM at $V_{\text{pg}}^{\text{GM}} = 1.2$ mV, the electrons form a state accumulated in the dots with a strong electron tunneling between the dots similar to the charge density distribution in the x -polarization shown in Fig. 9(d). Thus, the current in the GM is higher than that in the FES.

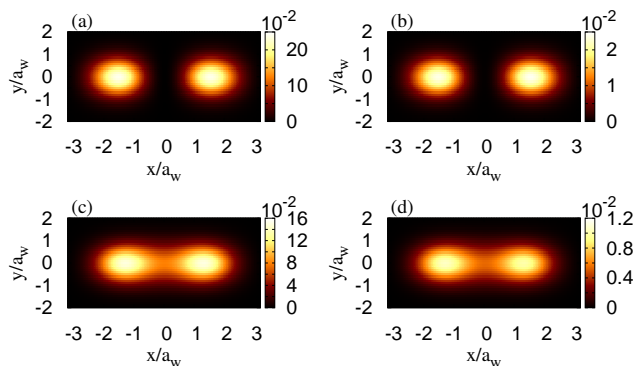


FIG. 11. (Color online) The charge density distribution of the DQD system with y -polarized photon field at time 220 ps corresponding to (a) photon-induced first-excited side-peak $V_{\text{pg}}^{\text{FES}} = 0.55$ mV, (b) first-excited main-peak $V_{\text{pg}}^{\text{FEM}} = 0.8$ mV, (c) photon-induced ground-state side-peak $V_{\text{pg}}^{\text{GS}} = 0.95$ mV, and (d) ground-state main-peak $V_{\text{pg}}^{\text{GM}} = 1.2$ mV of Fig. 10 for the case of $g_{\text{ph}} = 0.1$ meV (blue solid line). Other parameters are $\hbar\omega_{\text{ph}} = 0.25$ meV, $B = 0.1$ T, $a_w = 23.8$ nm, $L_x = 300$ nm, and $\hbar\Omega_0 = 2.0$ meV.

IV. CONCLUSIONS

Photon-assisted transient electron transport through a DQD system placed in a photon cavity with initially two linearly polarized photons can be controlled by a plunger-gate voltage. The serial double quantum dot molecule is important since the two lowest states of it have very different properties reflected in the fact that the wave-function of one is symmetric, but antisymmetric of the other.

We analyzed the electron transport through the system without and with a photon cavity by using a non-Markovian QME formalism. In the absence of a photon cavity, two current peaks were found: Ground state peak and a peak due to the first-excited state, originating from resonance energy levels of the DQD system with the first-subband energy of the leads. These two states could be used for a qubit in a quantum computer, in which the ground state resonance exhibits a strong inter-dot electron tunneling while the electrons in the first-excited state resonance form a state localized in each dot.

In the presence of either longitudinally or transversely polarized cavity photon field, two extra side-peaks are found: A peak due to the photon-replica of the ground state, and a photon replica of the first-excited state. The appearance of side-peaks is due to PAT of electrons in the DQD system. The characteristics of the photon activated MB states have been used to analyze the nature of the PAT. The peak due to the photon-replica of ground state is caused by multiphoton absorption processes with up to three photons. In the peak caused by the photon replica of the first-excited state, the electrons in the leads are transferred to two-photons states in the DQD system accumulation charge in the individual dots

without inter-dot tunneling. Furthermore, the current in the photon-induced side-peaks is strongly enhanced by increasing electron-photon coupling strength in the x -polarized of the photon field, while a very slightly enhancement in the photon-induced side-peak current was observed in the y -polarization photon. This discrepancy between the polarizations is explained by the anisotropy of the confinement of the central system.

Change in the photon-electron coupling strength alters the inter-dot tunneling sensitively, altering the conduction through the system. To describe this effect properly it is important to include many higher energy states in the system. Along the similar line of thought our calculations show that in the present system photon processes of more than one photon are important.

The fact that we include both the para- and diamagnetic terms in the electron-photon interaction leads to complex photon-electron processes that all contribute to the PAT resonance peaks observed. This has to be viewed in light of the common practice to use only the paramagnetic part in two-level systems in order to calculate PAT phenomena. In many systems the geometry matters, and the both parts of the interaction can be important for strong enough coupling.

ACKNOWLEDGMENTS

This work was financially supported by the Icelandic Research and Instruments Funds, the Research Fund of the University of Iceland, the Nordic High Performance Computing facility in Iceland, and the National Science Council in Taiwan through Contract No. NSC100-2112-M-239-001-MY3.

* nra1@hi.is

† cstang@nuu.edu.tw

‡ vidar@raunvis.hi.is

¹ G. Wailfred, v. d. Wiel, T. Fujisawa, S. Tarucham, and L. P. Kouwenhoven, *Jpn. J. Appl. Phys.* **40**, 2100 (2001).

² W. G. van der Wiel, S. De Franceschi, J. M. Elzerman, T. Fujisawa, S. Tarucham, and L. P. Kouwenhoven, *Reviews of modern physics* **75** (2003).

³ N. R. Abdullah, C. S. Tang, A. Manolescu, and V. Gudmundsson, *Journal of Physics:Condensed Matter* **25**, 465302 (2013).

⁴ M. Bagheri Tagani and H. Rahimpour Soleimani, *Physica B: Condensed Matter* **413**, 86:91 (2013).

⁵ C. Xu and M. G. Vavilov, *Phys. Rev. B* **87**, 035429 (2013).

⁶ F. M. Souza, T. L. Carrara, and E. Vernek, *Phys. Rev. B* **84**, 115322 (2011).

⁷ J. Wätzel, A. S. Moskalenko, and J. Berakdar, *Appl. Phys. Lett.* **99**, 192101 (2011).

⁸ G. Muñoz Matutano, M. Royo, J. I. Climente, J. Canet-Ferrer, D. Fuster, P. Alonso-González, I. Fernández-

Martínez, J. Martínez-Pastor, Y. González, L. González, F. Briones, and B. Alén, *Phys. Rev. B* **84**, 041308 (2011).

⁹ P. Kaczmarkiewicz, P. Machnikowski, and T. Kuhn, *Journal of Applied Physics* **114**, 183108 (2013).

¹⁰ C. A. Stafford and N. S. Wingreen, *Phys. Rev. Lett.* **76**, 1916 (1996).

¹¹ T. H. Stoof and Y. V. Nazarov, *Phys. Rev. B* **53**, 1050 (1996).

¹² R. Shang, H.-O. Li, G. Gao, M. Xiao, T. Tu, H. Jiang, G.-C. Guo, and G.-P. Guo, *Appl. Phys. Lett.* **103**, 162109 (2013).

¹³ K. Shibata, A. Umeno, K. M. Cha, and K. Hirakawa, *Phys. Rev. Lett.* **109**, 077401 (2012).

¹⁴ A. Imamoglu and Y. Yamamoto, *Phys. Rev. Lett.* **72**, 210 (1994).

¹⁵ D. Loss and D. P. DiVincenzo, *Physical Review A* **57**, 120 (1998).

¹⁶ D. P. DiVincenzo, *Science* **309** (2005).

¹⁷ L. I. Chuang and M. A. Nielsen, *Quantum Computation and Quantum Information* (Cambridge University Press,

- 2010).
- ¹⁸ E. Vaz and J. Kyriakidis, Phys. Rev. B **81**, 085315 (2010).
- ¹⁹ S. A. Gurvitz and Y. S. Prager, Phys. Rev. B **53**, 15932 (1996).
- ²⁰ U. Harbola, M. Esposito, and S. Mukamel, Phys. Rev. B **74**, 235309 (2006).
- ²¹ N. G. Van Kampen, *Stochastic Processes in Physics and Chemistry 2nd Ed* (North-Holland, Amsterdam, 2001).
- ²² A. Bednorz and W. Belzig, Phys. Rev. Lett. **101**, 206803 (2008).
- ²³ A. Braggio, J. König, and R. Fazio, Phys. Rev. Lett. **96**, 026805 (2006).
- ²⁴ C. Emary, D. Marcos, R. Aguado, and T. Brandes, Phys. Rev. B **76**, 161404 (2007).
- ²⁵ V. Gudmundsson, C. Gainar, C.-S. Tang, V. Moldoveanu, and A. Manolecu, New J. Phys. **11**, 113007 (2009).
- ²⁶ N. R. Abdullah, C.-S. Tang, and V. Gudmundsson, Phys. Rev. B **82**, 195325 (2010).
- ²⁷ C. Yannouleas and U. Landman, Rep. Prog. Phys **70**, 2067 (2007).
- ²⁸ V. Gudmundsson, O. Jonasson, C.-S. Tang, H.-S. Goan, and A. Manolescu, Phys. Rev. B **85**, 075306 (2012).
- ²⁹ V. Gudmundsson, O. Jonasson, T. Arnold, C.-S. Tang, H.-S. Goan, and A. Manolescu, Fortschr. Phys. **61**, 305 (2013).
- ³⁰ J. S. Jin, X. Zheng, and Y. Yan, J. Chem. Phys. Lett. **128**, 234703 (2008).
- ³¹ F. Haake, Phys. Rev. A **3**, 1723 (1971).
- ³² H.-P. Breuer and F. Petruccione, *The Theory of Open Quantum Systems* (Oxford University Press, Oxford, 2002).
- ³³ L. P. Kouwenhoven, S. Jauhar, J. Orenstein, P. L. McEuen, Y. Nagamune, J. Motohisa, and H. Sakaki, Phys. Rev. Lett. **73**, 3443 (1994).
- ³⁴ G. Platero and R. Aguado, Physics Report **395**, 1 (2004).